arXiv:1403.5857v2 [cond-mat.supr-con] 25 Mar 2014

Majorana edge states and topological properties in 1D/2D Rashba semiconductor proximity coupled to iron-based superconductor

Hiromi Ebisu[1], Keiji Yada[2], Hideaki Kasai[1,3], and Yukio Tanaka[2]

[1]*Department of Applied Physics, Osaka University, 2-1 Yamadaoka, Suita, Osaka 565-0871, Japan*

[2]*Department of Applied Physics, Nagoya University, Nagoya 464-8603, Japan*

[3]*Center for Atomic and Molecular Technologies, Osaka University, 2-1 Yamadaoka, Suita, Osaka 565-0871, Japan*

We study Majorana edge states and their topological properties of one-dimensional(1D) and two-dimensional(2D) Rashba semiconductor deposited on iron-based superconductor under the applied Zeeman field for various directions. Using the recursive Green's function method, we calculate the local density of states(LDOS) both for $s_{\pm}$ and s_{++}-wave pairings. We elucidate that it shows anisotropic response to the applied Zeeman field specific to Majorana edge states. This anisotropy can be understood by the winding number, which shows whether the present system is topological or not. The resulting LDOS and winding numbers for $s_{\pm}$ and s_{++}-wave pairings are significantly different at the lower Zeeman field. These results serve as a guide to determine the pairing symmetry of iron-pnictide.

1. Introduction

Topological superconducting systems with gapless surface Andreev bound states (SABSs) are focused in condensed matter physics now.[1–4] In these systems, Majorana fermions[1,3,5,6] appear as SABSs or vortex core states. For the future application of a fault tolerant quantum computation, Majorana fermions are important ingredients[7] since they obey non-Abelian statistics. Topological superconductivity with Majorana fermions was originally discussed in spinless triplet p-wave superconductors.[1,6,8] However, to realize spinless triplet superconductor is not easy in real solid state systems.

Fu and Kane proposed that topological superconductivity is possible in ferromagnet / spin-singlet s-wave superconductor hybrid system deposited on the surface of topologi-

cal insulator.[9] To elucidate the physical properties of Majorana fermions in this system has become a hot topic and several theoretical[10–13] and experimental researches[14,15] have been presented. The key concept for the generation of topological superconductivity from conventional spin-singlet s-wave superconductor is the simultaneous existence of spin-orbit coupling and the broken time reversal symmetry like Zeeman field.[16,17] In the presence of the Rashba spin-orbit coupling, the energy dispersion of free electrons splits into two. Further, by introducing Zeeman field and tuning chemical potential, one of the spin-polarized Fermi surface disappears. Then, exotic spinless metallic state, i.e. helical metallic state, is attainable where the direction of the spin of an electron is rocked to the momentum.

A semiconductor quantum well coupled to an s-wave superconductor and a ferromagnetic insulator is a possible candidate,[18,19] where one-dimensional chiral Majorana edge state is generated as a SABS. Also Majorana edge state was proposed in semiconductor nano-wires deposited on the surface of spin-singlet s-wave superconductor in the presence of external Zeeman field.[20,21] Since Majorana edge state is generated as the end state of the nano-wire, braiding operation might be possible by making network of wires.[22] It is noted that several experiments supported the existence of Majorana edge state[23–28] through zero bias conductance peak[29–34] or anomalous Josephson current.[35,36]

Besides these streams, there have been many researches about topological superconductivity in the time-reversal invariant (TRI) systems without the Zeeman field.[37–49] These systems belong to so called DIII class in the periodic table[37] of topological materials. Doped topological insulator Bi_2Se_3 is one of the candidate materials of DIII class superconductor.[50,51] Although several theoretical and experimental works support the realization of TRI topological superconductivity in this material, pairing symmetry and resulting Majorana modes are not fully determined yet.

There are several proposals to realize TRI topological superconductors (SCs) based on hybrid systems proximity coupled to unconventional superconductors.[49,52,53] Recently, Zhang, Kane and Mele proposed hybrid systems combining doped Rashba semiconductors (RSs) and iron-based SCs.[54] They have assumed that spin-singlet $s_{\pm}$-wave pairing is realized in iron-based SCs.[55–57] Then, the resulting pair potential in semiconductor has a sign change between Γ and M points. Kramers pair of Majorana edge states is generated at the boundary of the 2D (1D) TRI hybrid superconducting system due to the sign change of the pair potential between the two Fermi surfaces. However, the pairing symmetry of the iron based superconductors is still in the hot debate. So

called s_{++}-wave pairing with no sign change of the pair potential is also possible by the orbital fluctuation.[58–60] Although, tunneling spectroscopy of iron-based superconductors have been calculated,[61,62] the significant qualitative difference of the line shape of the tunneling conductance between $s_{\pm}$-wave and s_{++}-wave pairing does not exist. The tunneling conductance of normal metal / $s_{\pm}$-wave superconductor junctions is not distinct as compared to d-wave[29,30] or p-wave.[63–66] superconductor junctions. Thus, it is highly encouraged to present a new idea to distinguish above two parings in a qualitative level.

In the present paper, we study 1D/2D edge states of doped Rashba semiconductor deposited on iron-based superconductors by applying the Zeeman field for various directions. Using recursive Green's function method, we calculate local density of states on the edge and the angle resolved local density of states in two-dimensional case both for $s_{\pm}$ and s_{++}-wave paring cases. We concentrate on the Majorana edge modes as an ABS and relevant local density of state (LDOS) including zero energy peak (ZEP). We elucidate that the anisotropic response to the Zeeman field stems from the mirror reflection symmetry.[67–71] We also calculate winding numbers of the Hamiltonian and analyze topological properties. The resulting LDOS and winding numbers are seriously different between these two pairing cases. It can be concluded that Rashba semiconductor / iron-based superconductor hybrid junctions are useful to determine the pairing symmetry of iron-pnictide.

The organization of this paper is as follows. In section 2, we explain the model, Hamiltonian, and the formulation. In section 3.1, we study a 1D Rashba semiconductor nanowire / iron-based superconductor hybrid system. We calculate energy spectrum of the bulk nanowire and LDOS on the edge for various directions of the applied Zeeman field. In section 3.2, we study a 2D Rashba semiconductor layer / iron-based superconductor hybrid system. Angle resolved LDOS for fixed momentum k_y parallel to the surface and angle averaged LDOS on the edge are calculated. Both in 3(a) and 3(b), we compare the results of $s_{\pm}$-wave and s_{++}-wave case. In section 4, we interpret calculated results in section 3 based on winding number of the system. We also discuss the reason why LDOS is sensitive to the direction of the applied Zeeman field in terms of the Ising like spin of Majorana edge sate. In section 5, we summarize our results.

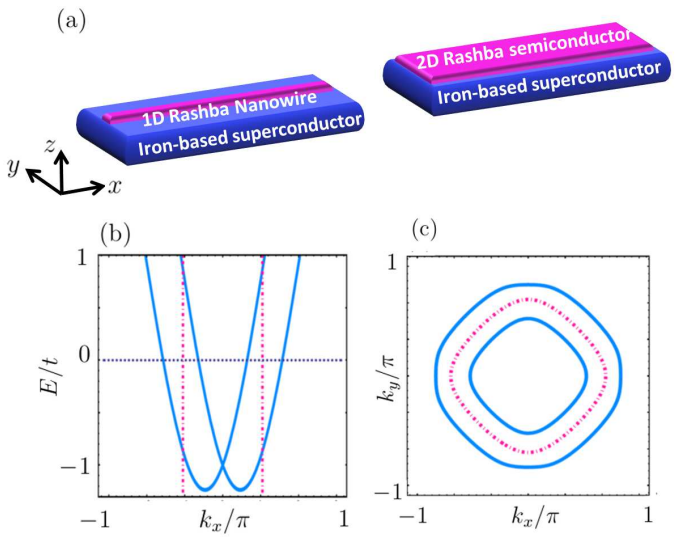

Fig. 1. (a)(left)A 1D Rashba semiconductor nanowire(left) and a 2D Rashba semiconductor layer(right) deposited on iron-based superconductors.(b) The energy dispersion of a nanowire in the normal state for t=1, $\lambda_R = 0.5$ (solid line) and the position of Fermi energy $\mu = -1$ (dotted line). Dot-dashed line denotes nodal lines for $\Delta_0 = -0.2$, $\Delta_1 = 0.2$. The sign of the pair potential inside(outside) nodal lines is positive(negative). (c)Fermi surface of a Rashba layer for t=1, $\lambda_R = 0.5$, and $\mu = -1$ (solid line). Dot-dashed line denotes nodal line for $\Delta_0 = -0.2$, $\Delta_1 = 0.2$.

2. Formulation

In this section, we introduce model Hamiltonian of 1D and 2D Rashba semiconductors deposited on iron-based superconductors as shown in Fig. 1(a) and write a formula of recursive Green's function to calculate LDOS on the edge.

2.1 Model

Model Hamiltonian of 1D Rashba doped semiconductor nanowire in momentum space reads

$$\begin{aligned} \mathcal{H}_0^{\rm 1D}(k_x) &= (-2t\cos k_x - \mu)\sigma_0\tau_z + 2\lambda_R \sin k_x \sigma_y\tau_z \\ &\quad -\Big(\Delta_0 + 2\Delta_1 \cos k_x\Big)\sigma_y\tau_y, \end{aligned} \tag{1}$$

where t is the nearest neighbor hopping, μ is a chemical potential, λ_R is Rashba spin-orbit coupling. We have chosen the value of chemical potential μ, so that charge transport properties of Rashba semiconductor becomes metallic by doping effect. Δ_0 and Δ_1 are proximity induced pair potentials in 1D Rashba semiconductor. In general, these values are less than that in bulk iron-based superconductor. σ and

τ are the Pauli matrices in spin space and electron-hole space, respectively. When $|\mu - t\Delta_0/\Delta_1| < 2\lambda_R\sqrt{1-\Delta_0^2/(4\Delta_1^2)}$, quasiparticle feels different sign of pair potential at the inner and the outer Fermi points. Then, we verify that $s_\pm$-wave pairing is realized in the 1D Rashba semiconductor.

The corresponding model Hamiltonian of 2D Rashba semiconductor in momentum space is given by

$$\begin{aligned}\mathcal{H}_0^{\rm 2D}(k_x,k_y) &= \Big(-2t(\cos k_x+\cos k_y)-\mu\Big)\sigma_0\tau_z \\ &\quad -2\lambda_R\sin k_y\sigma_x\tau_0+2\lambda_R\sin k_x\sigma_y\tau_z \\ &\quad -\Big(\Delta_0+2\Delta_1(\cos k_x+\cos k_y)\Big)\sigma_y\tau_y \end{aligned} \tag{2}$$

When we choose $|\mu - t\Delta_0/\Delta_1| < 2\lambda_R\sqrt{2-\Delta_0^2/(8\Delta_1^2)}$, $s_\pm$-wave pairing is realized.

The nodal lines for $s_\pm$-wave case in 1D and 2D are shown in Figs. 1(b) and (c), respectively. For $s_\pm$-wave pairing, Majorana Kramers Doublets emerge as edge states, and DIII class topological superconducting state is realized.[54] The applied Zeeman field is given by

$$\hat{V}_i = \begin{cases} V_x\sigma_x\tau_z \ (i=x,\ x\text{-direction}) \\ V_y\sigma_y\tau_0 \ (i=y,\ y\text{-direction}) \\ V_z\sigma_z\tau_z \ (i=z,\ z\text{-direction}). \end{cases} \tag{3}$$

Thus, the total Hamiltonian in 1D and 2D with the Zeeman field is given by

$$\mathcal{H}_i^{\rm 1D(2D)}(k_x(k_x,k_y)) = \mathcal{H}_0^{\rm 1D(2D)}(k_x(k_x,k_y)) + \hat{V}_i. \tag{4}$$

In the presence of the Zeeman field, the time-reversal symmetry is broken and topological nature of the Majorana edge states is changing.

2.2 Recursive Green's function

First, we derive a general formula of the recursive Green's function in 1D. Consider a system which has finite length in the x-direction. Suppose the number of the sites is N_x, and add one more site in the x-direction (Fig. 2(a)). Based on the Dyson equation, we obtain

$$G = G_0 + G_0TG \tag{5}$$

for Green's function G of this system, where

$$G_0 = |N_x\rangle\, G_{N_x,N_x}\, \langle N_x| + |N_x+1\rangle\, g_{\rm iso}\, \langle N_x+1|$$

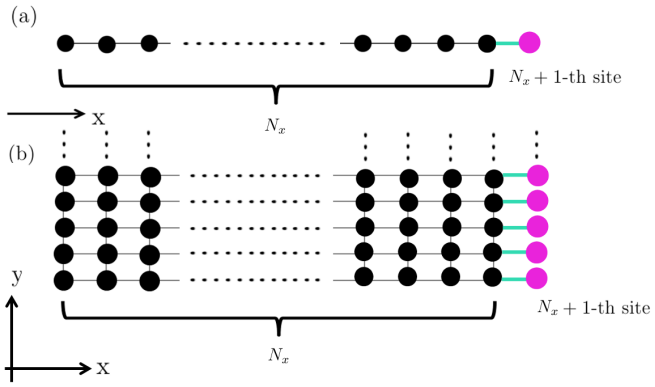

Fig. 2. Schematic pictures of the process of calculating recursive Green's function in (a)1D case and (b)2D case.

$$T = |N_x+1\rangle\, T_{N_x+1,N_x}\, \langle N_x| + h.c. \tag{6}$$

G_{N_x,N_x} is the Green's function at N_x-site, g_{iso} is the isolated Green's function at N_x+1-site, and $T_{N_x+1,N_x(N_x,N_x+1)}$ is a transfer integral from N_x-th to N_x+1-th (N_x+1 to N_x) site. We derive following two equations from Eq. (5),

$$G_{N_x+1,N_x+1} = g_{\rm iso} + g_{\rm iso} T_{N_x+1,N_x} G_{N_x,N_x+1} \tag{7}$$

$$G_{N_x,N_x+1} = G_{N_x,N_x} T_{N_x,N_x+1} G_{N_x+1,N_x+1}. \tag{8}$$

By substituting G_{N_x,N_x+1} in (7) for (8), we obtain

$$G_{N_x+1,N_x+1} = \left(g_{\rm iso}^{-1} - T_{N_x+1,N_x} G_{N_x,N_x} T_{N_x,N_x+1}\right)^{-1} \tag{9}$$

Once we know G_{N_x,N_x}, we obtain G_{N_x+1,N_x+1}. In order to calculate the LDOS, we evaluate a retarded Green's function $G_{jj}(E+i0^+)$ with site index j and energy E measured from the Fermi level, where 0^+ is an infinitesimal number. In the present model, following relations

$$T_{j+1,j} = -t\sigma_0\tau - i\lambda_R\sigma_y\tau_z - \Delta_1\sigma_y\tau_y \;\; (j = 1 \sim N_x) \tag{10}$$

$$g_{\rm iso}(E) = \left(EI_{4\times4} - \mathcal{H}_{\rm iso}\right)^{-1} \tag{11}$$

$$\mathcal{H}_{\rm iso} = -\mu\sigma_0\tau_z - \Delta_0\sigma_y\tau_y + \hat{V}_i, \tag{12}$$

are satisfied. After calculating $G_{1,1}(E) = g_{\rm iso}(E)$, we can obtain Green's function of any number of sites in the x-direction. Finally, LODS on the edge is give by

$$\rho^{\rm 1D}(E) = -\frac{1}{\pi}{\rm Im}\Big\{{\rm Tr}[G_{N_x+1,N_x+1}(E+i0^+)]\Big\}, \tag{13}$$

where Im denotes to choose imaginary part. In the evaluation of the trace of $G_{N_x+1,N_x+1}(E+i0^+)$, we sum up only the electronic part of $G_{N_x+1,N_x+1}(E+i0^+)$.

In the 2D model, we assume that the boundary is flat as shown in Fig.2(b). In this case, momentum k_y is a good quantum number. Then, we can calculate the recursive Green's function for each k_y in the similar way in 1D case. We obtain

$$T_{i+1,i} = -t\sigma_0\tau - i\lambda_R\sigma_y\tau_z - \Delta_1\sigma_y\tau_y \ \ (i = 1 \sim N) \tag{14}$$

$$g_{\rm iso}(E, k_y) = \Big(EI_{4\times4} - \mathcal{H}_{\rm iso}(k_y)\Big)^{-1} \tag{15}$$

$$\begin{aligned}\mathcal{H}_{\rm iso}(k_y) = \Big(-2t(\cos k_x + \cos k_y) - \mu\Big)\sigma_0\tau_z \\ -2\lambda_R \sin k_y \sigma_x\tau_0 \\ -\Big(\Delta_0 + 2\Delta_1\cos k_y\Big)\sigma_y\tau_y + \hat{V}_i.\end{aligned} \tag{16}$$

Angle resolved local density of states (ARLDOS) for each k_y is given by

$$D^{\rm 2D}(E, k_y) = -\frac{1}{\pi}{\rm Im}\Big\{{\rm Tr}[G_{N_x+1,N_x+1}(E+i0^+, k_y)]\Big\}. \tag{17}$$

To obtain the LDOS, we calculate

$$\rho^{\rm 2D}(E) = \frac{1}{N_y}\sum_{k_y} D^{\rm 2D}(E, k_y), \tag{18}$$

where, N_y is a number of sites in the y-direction. Using Eqs. (13), (17), and (18), we obtain LDOS on the edge of 1D model and ARLDOS and LDOS in the 2D model in the presence of the Zeeman field (x, y, z-directions) both for $s_\pm$ and s_{++}-wave pairing.

3. Calculated results of LDOS

In this section, we show the results of LDOS in 1D and ARLDOS and LDOS in 2D. In this paper, we fix parameters as t=1, $\lambda_R = 0.5$, $\mu = -1$. We choose $\Delta_0 = -0.2$ and $\Delta_1 = 0.2$ for $s_\pm$-wave pairing and $\Delta_0 = 0.2$ and $\Delta_1 = 0$ for s_{++}-wave pairing.

3.1 1D Rashba semiconductor

First, we show the LDOS on the edge of a 1D Rashba semiconductor nanowire deposited on iron-based superconductors with the Zeeman field in the x, y, and z-directions for $s_\pm$-wave case (Fig. 3). Due to the presence of Majorana Kramers doublets realized without the Zeeman field, we can clearly see the zero energy peak of LDOS of edge state for $V_i = 0$ ($i = x, y, z$) (Fig. 3). Since this Kramers doublet is topologically protected by the time-reversal symmetry, a pair of Kramers doublet is lifted by the applied Zeeman field in general. Here, we show the LDOS under the applied Zeeman

field in the x, y and z-direction in Figs.3 (a), (b) and (c), respectively. A zero energy peak in the LDOS remains in the presence of the Zeeman field in the x and z-direction while it disappears for the y-direction. This suggests that remaining symmetry of the Hamiltonian, which is discussed below, protect the Majorana edge states under the Zeeman field in x and z-directions. Next, we see LDOS at the edge under the Zeeman field in the x-direction. We can also see a closing of the bulk energy gap at $V_x/t \sim 1$ and 3. A zero energy peak survives after the first gap closing at $V_x/t \sim 1$ as shown in Fig. 3(d). However, this zero energy peak disappears after the second gap closing at $V_x/t \sim 3$. The similar features are obtained when the Zeeman field is along z-direction.

In the case of s_{++}-wave pairing, no zero energy state (ZES), i.e., Majorana edge state, appears on the edge without the Zeeman field, but if we apply the Zeeman field in x, z-directions, LDOS has a ZEP at $V_{x,(z)}/t \sim 1$ (Fig. 4 (a)(c))[20,21] which is quite different from $s_{\pm}$-wave pairing case. When, we apply the Zeeman field in the y-direction, ZEP is not seen at all (Fig. 4(b)). These features are essentially the same with those in conventional s-wave superconductor / 1D Rashba semiconductor hybrid systems. For both $s_{\pm}$ and s_{++}cases, LDOS is sensitive to the direction of the Zeeman field. In the presence of the sufficient large magnitude of V_i $(i = x, y, z)$, LDOS has a ZES for $i = x$ and $i = z$ but not for $i = y$.

3.2 2D Rashba semiconductor

ARLDOS of 2D Rashba semiconductor on iron-based superconductor is shown in Figs. 5 to 10 both for $s_{\pm}$ and s_{++}-wave pairing cases. The resulting LDOS of $s_{\pm}$-wave and s_{++}-wave are shown in Figs. 11 and 12, respectively. Without the Zeeman field, helical edge modes crossing at $k_y = 0$ appear in $s_{\pm}$-wave pairing (Figs. 5(a),6(a),7(a)), while it does not in s_{++}-wave case (Figs. 8(a),9(a),10(a)). The resulting angular averaged LDOS $\rho^{2D}(E)$ at $E = 0$ has a nonzero value for $s_{\pm}$-wave pairing(solid lines in Fig. 11) while it becomes almost zero for s_{++}-wave pairing and has a typical U-shaped structure (solid lines in Fig. 12).

If we apply the Zeeman field, ARLDOS changes seriously. In the case of $s_{\pm}$-wave pairing, ARLDOS is very sensitive to the direction of the Zeeman field. When the applied Zeeman field is along the x-direction, the helical modes once disappear and ARLDOS at $k_y = E = 0$ is enhanced for $V_x = 0.5t$ shown in Figs. 5(b). The resulting LDOS has a zero energy enhanced structure shown by dashed line in Fig. 11(a). With the further increase of V_x, two chiral edge modes appear but are very close to continuum

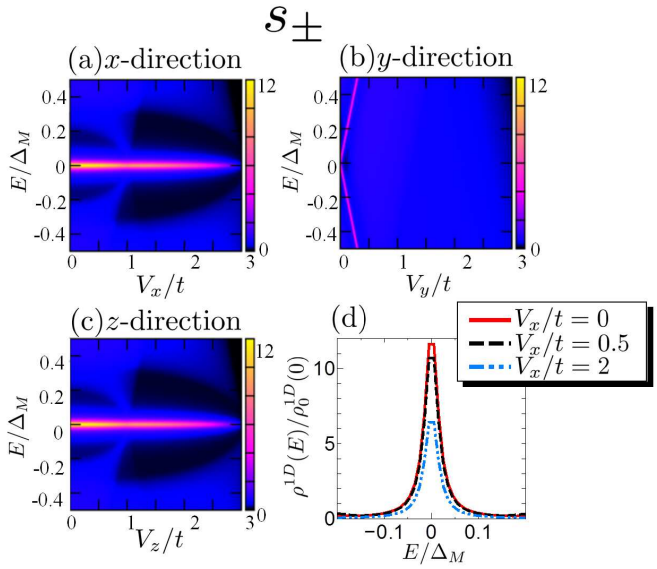

Fig. 3. (a)∼(c)Intensity plot of LDOS of a 1D Rashba semiconductor nanowire on $s_{\pm}$-wave superconductor with the Zeeman field in (a)x,(b) y, and (c)z-direction. (d)Normalized LDOS of a Rashba semiconductor nanowire on $s_{\pm}$-wave superconductor under the Zeeman field in the x-direction, for $V_x/t = 0$(solid line),$V_x/t = 0.5$(dashed line), $V_x/t = 2$(dot-dashed line). LDOS is normalized by its value in the normal state at $E = 0$, and the energy is normalized by $\Delta_M = \Delta_0 + 2\Delta_1$.

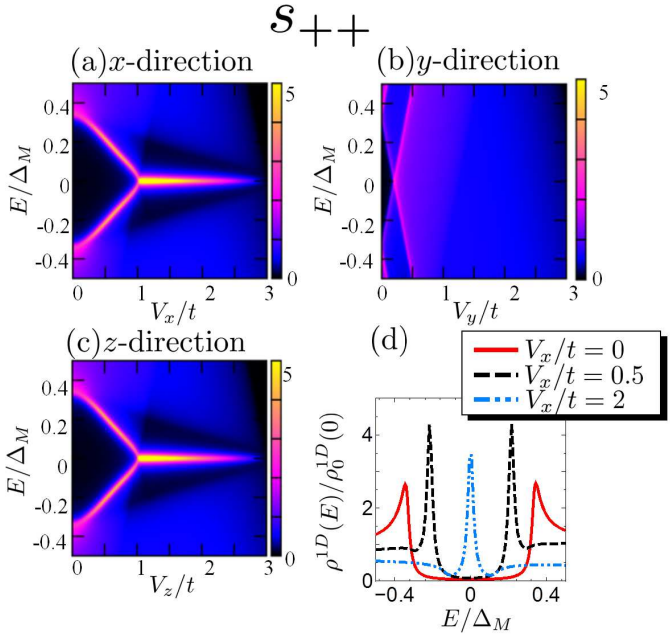

Fig. 4. (a)∼(c)Intensity plot of LDOS of a 1D Rashba semiconductor nanowire on s_{++}-wave superconductor with the Zeeman field in (a)x, (b)y, and (c)z-direction.(d)Normalized LDOS of a Rashba semiconductor nanowire on $s_{\pm}$-wave superconductor under the Zeeman field in the x-direction, for $V_x/t = 0$(solid line),$V_x/t = 0.5$(dashed line), $V_x/t = 2$(dot-dashed line). LDOS is normalized by its value in the normal state at $E = 0$, and the energy is normalized by $\Delta_M = \Delta_0 + 2\Delta_1$.

levels.[72] Then, the resulting LDOS has an almost flat curve without any structures as shown by dot-dashed line in Fig. 11(a). When the Zeeman field is applied in the y-direction, helical edge mode disappears simultaneously with gap closing and there is no clear edge mode any more. The resulting LDOS is almost insensitive to E as shown in Fig. 11(b). On the other hand, when the applied Zeeman field is along the z-direction, helical modes change into two chiral edge modes at $k_y = 0$ and $k_y = \pi$ (Fig. 7(d)) and then one of the chiral edge modes vanishes (Fig. 7(e)). Reflecting on the change of ARLDOS, the lines shapes of LDOS have fine structures shown by dot-dashed and dashed lines in Fig. 11 (c).

Next, we focus on s_{++}-wave pairing case where chiral Majorana edge mode is generated for the Zeeman field along the x and z-directions. In this case, Majorana edge mode appears only after the applied Zeeman field exceeds a critical value.[18–21] When the applied field is along the x-direction, although the edge mode appears, it is very near the continuum levels (Fig. 8(d)).[72] The line shape of the resulting LDOS does not have a sufficient change as a function of E shown in (dot-dashed line in Fig. 12 (a)). On the other hand, when the Zeeman field is applied in the y-direction, the bulk energy gap closes without any generation of the edge mode shown in Fig. 9. For the z-direction case, two chiral edge modes are generated at $k_y = 0$ and $k_y = \pi$ (Fig. 10(d)) and then one of the chiral edge mode vanishes (Fig. 10(e)). These features are similar to those in $s_{\pm}$-wave pairing case (Fig. 7).

To summarize, the resulting ARLDOS and LDOS are sensitive to the direction of the applied Zeeman field both for s_{++}-wave and $s_{\pm}$-wave pairings. The difference between $s_{\pm}$-wave and s_{++}-wave pairings becomes clear when the applied Zeeman field is along the z-direction with $0 < V_z/t < 1$ as seen from Figs. 7 and 10.

4. Symmetry of the Hamiltonian and topological invariants

In this section, we elucidate that the anisotropic response of LDOS and LDOS to the Zeeman field stems from the mirror reflection symmetry in 1D by introducing winding number.

4.1 1D case

In 1D case, the Hamiltonian belongs to DIII class in periodic table[37] and has time-reversal symmetry and particle-hole symmetries. In addition these two, the system has a mirror reflection symmetry. These symmetries are given as follows: (i) time-reversal

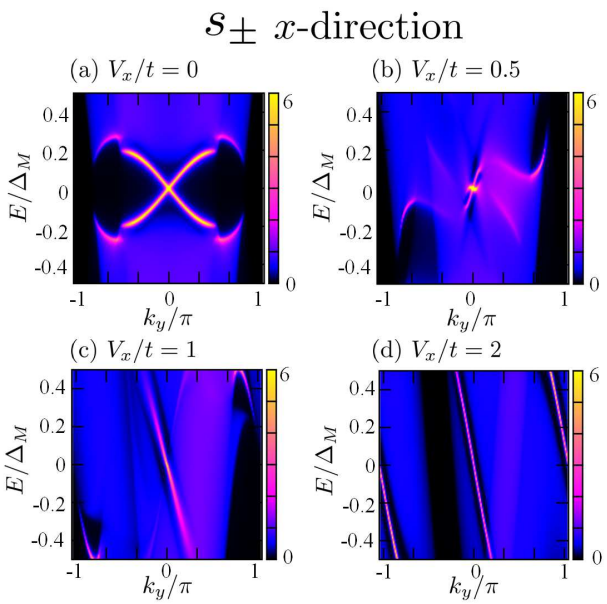

Fig. 5. ARLDOS of a 2D Rashba semiconductor layer in the case of $s_\pm$-wave pairing under the Zeeman field in the x-direction for V_x/t =(a)0, (b)0.5, (c)1, and (d)2. ARLDOS is normalized by its value in the normal state at $k_y = 0$ and $E = 0$. Energy is normalized by $\Delta_M = \Delta_0 + 4\Delta_1$.

symmetry

$$\Theta^\dagger \mathcal{H}_0^{1\mathrm{D}}(k_x)\Theta = (\mathcal{H}_0^{1\mathrm{D}}(-k_x))^*, \quad \Theta = -i\sigma_y\tau_0, \tag{19}$$

(ii)particle-hole symmetry

$$C^\dagger \mathcal{H}_0^{1\mathrm{D}}(k_x)C = -(\mathcal{H}_0^{1\mathrm{D}}(-k_x))^*, \quad C = \sigma_0\tau_x, \tag{20}$$

(iii)mirror reflection symmetry (mirror plane is xz-plane)

$$\mathcal{M}_{xz}^\dagger \mathcal{H}_0^{1\mathrm{D}}(k_x)\mathcal{M}_{xz} = \mathcal{H}_0^{1\mathrm{D}}(k_x), \quad \mathcal{M}_{xz} = i\sigma_y\tau_0. \tag{21}$$

Combining three symmetries together, we can define operator $\Gamma^{1D} = \mathcal{M}_{xz}\Theta C$ which anti-commutes with $\mathcal{H}_0^{1\mathrm{D}}(k_x)$.

$$\{\Gamma^{1\mathrm{D}}, \mathcal{H}_0^{1\mathrm{D}}(k_x)\} = 0. \tag{22}$$

Now, we consider the effect of the Zeeman field term $\hat{V}_i$ in Eq. (3). When the Zeeman field is applied in the x, z-directions, $\hat{V}_i$ anti-commutes with $\Gamma^{1\mathrm{D}}$.

$$\{\Gamma^{1\mathrm{D}}, \mathcal{H}_i^{1\mathrm{D}}(k_x)\} = 0, \quad i = x, z. \tag{23}$$

However, $\hat{V}_i$ does not anti-commute with $\Gamma^{1\mathrm{D}}$ when the direction of the Zeeman field is along the y-direction. If we find an operator which anti-commutes with Hamiltonian, i.e. the system has a chiral symmetry,[37] we can define winding number by following

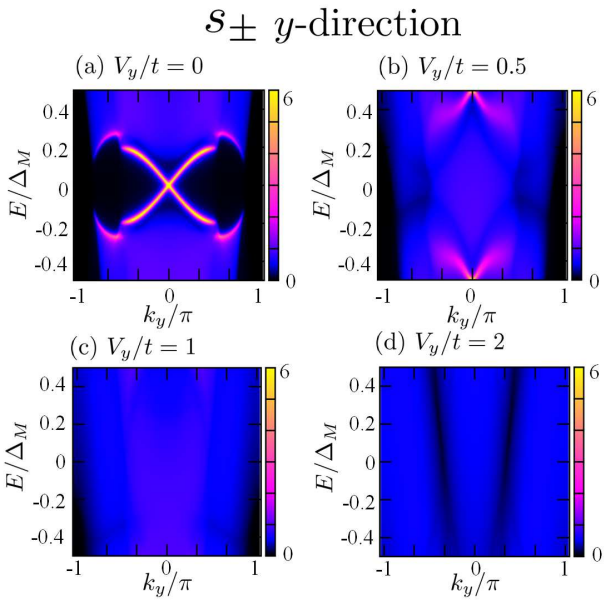

Fig. 6. ARLDOS of a 2D Rashba semiconductor layer in the case of $s_\pm$-wave pairing under the Zeeman field in the y-direction for V_y/t =(a)0, (b)0.5, (c)1, and (d)2. ARLDOS is normalized by its value in the normal state at $k_y = 0$ and $E = 0$. Energy is normalized by $\Delta_M = \Delta_0 + 4\Delta_1$.

procedures.[42,73,74] First, we diagonalize Γ^{1D} by the unitary matrix U_1

$$U_1^\dagger \Gamma^{1D} U_1 = \begin{pmatrix} I_{2\times 2} & 0 \\ 0 & -I_{2\times 2} \end{pmatrix}. \tag{24}$$

Using this U_1, the Hamiltonian is transformed as

$$U_1^\dagger \mathcal{H}_i(k_x) U_1 = \begin{pmatrix} 0 & q(k_x) \\ q(k_x)^\dagger & 0 \end{pmatrix}, \tag{25}$$

with $q(k_x) = (-2t\cos k_x - \mu)\sigma_0 + 2\lambda \sin k_x \sigma_y - i(\Delta_0 + 2\Delta_1 \cos k_x)\sigma_y$. The winding number w_{1d} is defined as

$$w_{1d} = \frac{1}{2\pi i} \oint D^{-1} dD, \quad D = \det q(k_x), \tag{26}$$

where $\oint$ represents the line integral over closed loop in 1D Brillouin zone.[73] This quantity means how many times the trajectory of the $\det q(k_x) = m_1 + i m_2$ wraps around the origin in complex space, where m_1 and m_2 are real quantities. The number w_{1d} is a topological invariant, which keeps its value unless the energy gap of the Hamiltonian is closed. If w_{1d} has a non-zero value, due to the bulk-edge correspondence, there are ZESs.[73] As an example, we plot trajectories of det $q(k_x)$ in complex m_1-m_2 plane and the energy dispersion of $\mathcal{H}_d^{1D}(k_x)$ in the case of $s_\pm$-wave pairing without the Zeeman

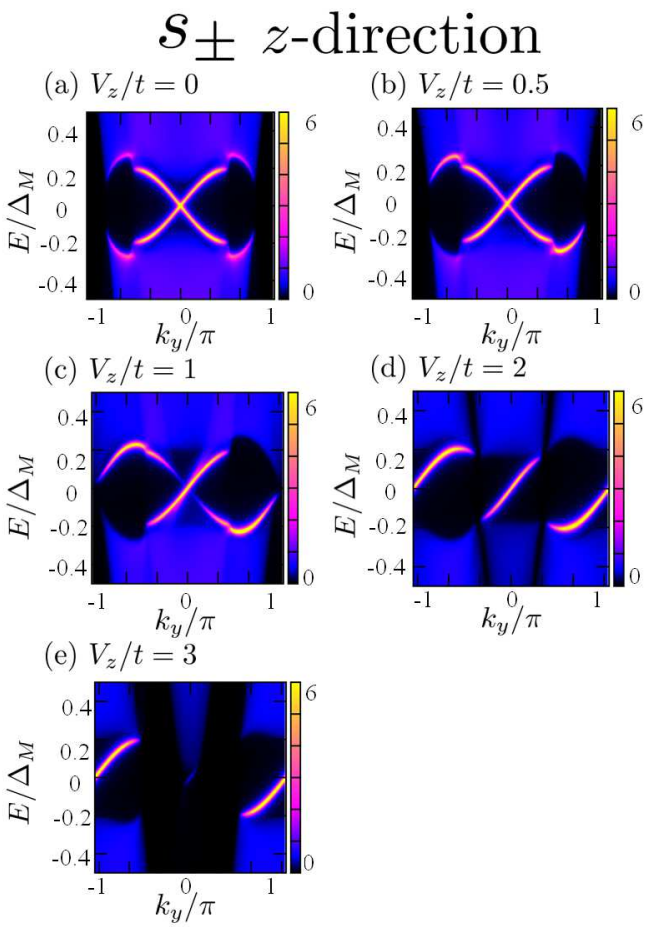

Fig. 7. ARLDOS of a 2D Rashba semiconductor layer in the case of $s_\pm$-wave pairing under the Zeeman field in the z-direction for $V_z/t =$(a)0, (b)0.5, (c)1, (d)2, and (e)3. ARLDOS is normalized by its value in the normal state at $k_y = 0$ and $E = 0$. Energy is normalized by $\Delta_M = \Delta_0 + 4\Delta_1$.

field (Figs. 13 (a) and (b)) and with it (Figs. 13 (c), (d) (e) and (f)). We can easily find $w_{1d} = 2$ without the Zeeman field as shown in Fig. 13 (a). w_{1d} remains to be 2 up to $V_x = V_{c1}$ ($V_{c1}/t \sim 1.02$) which is the critical value of the bulk energy gap closure. At $V_x = V_{c1}$, the trajectory just crosses $(m_1, m_2) = (0, 0)$ (Fig. 13(c)) and bulk energy gap closes at $k_x = 0$ (Fig. 13(d)). If V_x exceeds V_{c1}, the resulting w_{1d} becomes 1. At $V_x = V_{c2}$, with $V_{c2}/t \sim 3.06$, the trajectory crosses $(m_1, m_2) = (0, 0)$ (Fig. 13 (e)) and the bulk energy gap closes at $k_x = \pm\pi$ (Fig. 13(f)). Above V_{c2}, w_{1d} becomes zero. These properties are consistent with that the topological invariant w_{1d} changes when the bulk energy gap is closed. We also calculate w_{1d} under the Zeeman field in the z-direction for $s_\pm$-wave pairing. The change of w_{1d} and critical values of V_{c1} and V_{c2} are the same as in the case with the Zeeman field in the x-direction. As a reference, we obtain w_{1d} for s_{++}-wave pairing with the Zeeman field both in x and z-directions. In these directions,

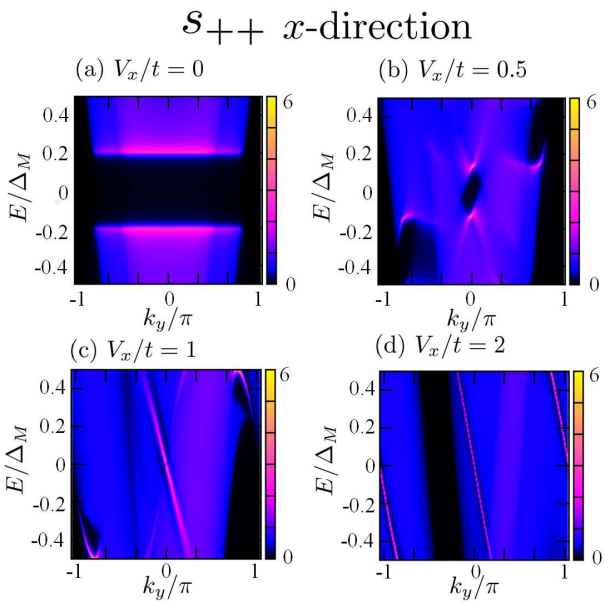

Fig. 8. ARLDOS of a 2D Rashba semiconductor layer in the case of s_{++}-wave pairing under the Zeeman field in the x-direction for V_x/t =(a)0, (b)0.5, (c)1, and (d)2. ARLDOS is normalized by its value in the normal state at $k_y = 0$ and $E = 0$. Energy is normalized by $\Delta_M = \Delta_0 + 4\Delta_1$.

w_{1d} changes 0, 1, 0 with the increase of the Zeeman field. The critical values V_{c1} and V_{c2} are given as $V_{c1} \sim 1.02$ and $V_{c2} \sim 3.00$, respectively. The above results are shown in Table I. The arrow in the Table 1 shows the change of the topological numbers with the increase of the Zeeman field.

Pairing	x-direction	y-direction	z-direction
$s_{\pm}$	$2 \to 1 \to 0$	$\times$	$2 \to 1 \to 0$
s_{++}	$0 \to 1 \to 0$	$\times$	$0 \to 1 \to 0$

Table I. Changes of w_{1d} in 1D with the increase of Zeeman field. The critical values of the Zeeman field where, the winding number is changed, are mentioned in Appendix. A.

From this table, it is clear that the difference between $s_{\pm}$ and s_{++}-wave pairings is whether the state with $w_{1d} = 2$ is realized or not at the lower Zeeman field in the x and z-direction. This point is also clearly seen in Figs. 4 and 5. Up to $V_x = V_{c1}$, ZES and resulting ZEP appear in the LDOS on the edge only for $s_{\pm}$-wave pairing. The response of the w_{1d} to the Zeeman field is seriously different between $s_{\pm}$ and s_{++}-wave pairing.

Next, we mention the anisotropic response of LDOS to the applied Zeeman field. To understand this, both the time-reversal and the mirror reflection symmetries are

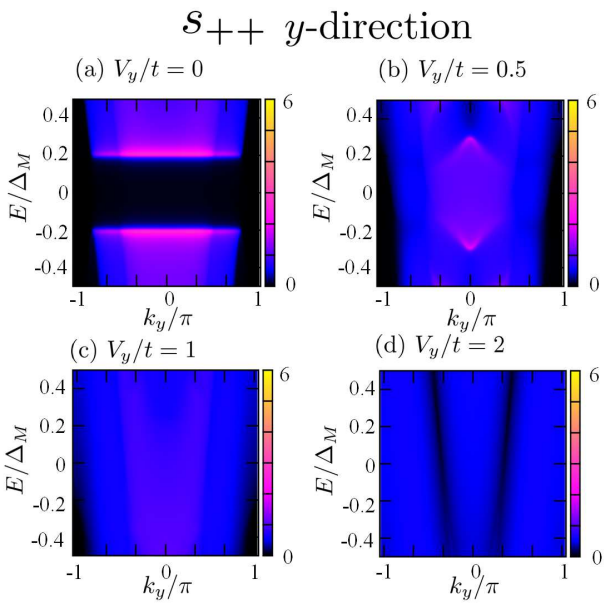

Fig. 9. ARLDOS of a 2D Rashba semiconductor layer in the case of s_{++}-wave pairing under the Zeeman field in the y-direction for V_y/t =(a)0, (b)0.5, (c)1, and (d)2. ARLDOS is normalized by its value in the normal state at $k_y = 0$ and $E = 0$. Energy is normalized by $\Delta_M = \Delta_0 + 4\Delta_1$.

essential. Suppose we have the Zeeman field term in the x-direction, $\hat{V}_x = V_x\sigma_x\tau_z$. This term breaks both the time-reversal symmetry and the mirror reflection symmetry,

$$\Theta^\dagger V_x\sigma_x\tau_z\Theta = -V_x\sigma_x\tau_z, \tag{27}$$

$$\mathcal{M}_{xz}^\dagger V_x\sigma_x\tau_z\mathcal{M}_{xz} = -V_x\sigma_x\tau_z. \tag{28}$$

However, there is the pseudo-time-reversal symmetry, i.e. the product of the time-reversal symmetry and the mirror reflection symmetry.

$$(\mathcal{M}_{xz}\Theta)^\dagger V_x\sigma_x\tau_z\mathcal{M}_{xz}\Theta = V_x\sigma_x\tau_z. \tag{29}$$

The Zeeman field in the z-direction also has this combined symmetry. In the presence

Direction	TR	MR	TR+MR
x-direction	×	×	◯
y-direction	×	◯	×
z-direction	×	×	◯

Table II. Symmetries of the Hamiltonian with the Zeeman field in the x,y, and z-directions. TR, MR, and TR+MR mean the time-reversal, mirror reflection, and pseudo-time-reversal symmetries, respectively. The symbol × (◯) represents that the corresponding symmetry is broken (not broken).

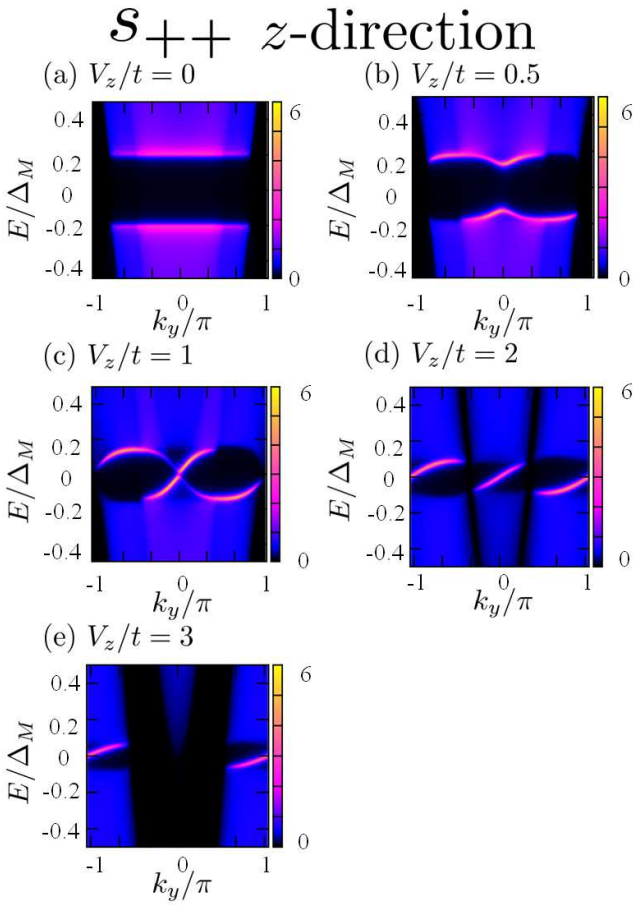

Fig. 10. ARLDOS of a 2D Rashba semiconductor layer in the case of s_{++}-wave pairing under the Zeeman field in the z-direction for $V_z/t =$(a)0, (b)0.5, (c)1, (d)2, and (e)3. ARLDOS is normalized by its value in the normal state at $k_y = 0$ and $E = 0$. Energy is normalized by $\Delta_M = \Delta_0 + 4\Delta_1$.

of this symmetry, we can define topological number and understand the origin of the edge state in the context of the bulk-edge correspondence.

Besides above discussions, we can provide another explanation about this anisotropic response to the Zeeman field by the index theorem. We focus on the zero energy edge state and analyze them by the eigenstate of $\Gamma^{\rm 1D}$. It is known that the index theorem guarantees the following relations[41] as

$$w_{1d} = n_0^+ - n_0^-, \tag{30}$$

or

$$w_{1d} = n_0^- - n_0^+, \tag{31}$$

where, $n_0^{+(-)}$ is a number of eigenstate of $\Gamma^{\rm 1D}$ whose eigenvalue is $+(-)1$.

Suppose Eq. (30) holds and $w_{1d} = 2$. ZES can be written as

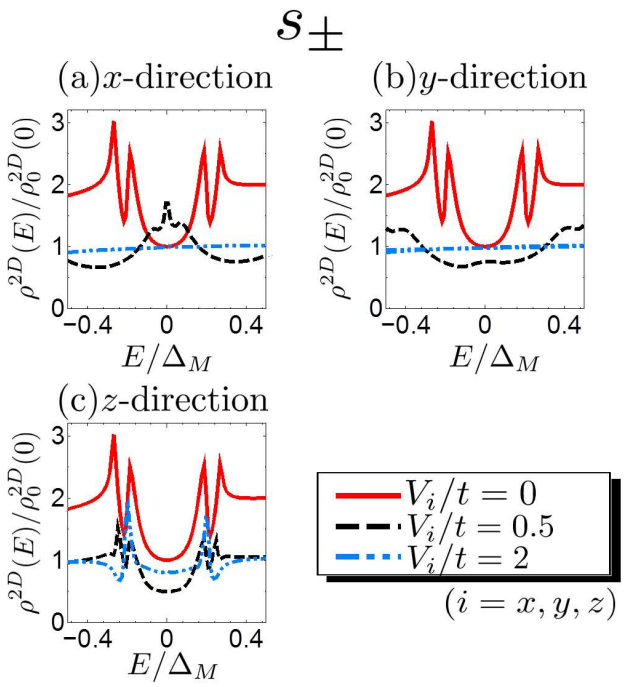

Fig. 11. (a)(b)(c)Normalized LDOS of a 2D Rashba semiconductor layer on $s_\pm$-wave superconductor with the Zeeman field $V_i/t = 0$ (solid line), $V_i/t = 0.5$ (dashed line), and $V_i/t = 2$ (dot-dashed line) in (a)x-direction, (b)y-direction, and (c)z-direction respectively. LDOS is normalized by its values in the normal state at $E = 0$.

$(\xi_\uparrow^{(a)}, \xi_\downarrow^{(a)}, \xi_\uparrow^{*(a)}, \xi_\downarrow^{*(a)})^T$ $(a = 1, 2)$ by using particle-hole symmetry. From $n_0^+ = 2$, it gives

$$\Gamma^{1D} \begin{pmatrix} \xi_\uparrow^{(a)} \\ \xi_\downarrow^{(a)} \\ \xi_\uparrow^{*(a)} \\ \xi_\downarrow^{*(a)} \end{pmatrix} = (+1) \begin{pmatrix} \xi_\uparrow^{(a)} \\ \xi_\downarrow^{(a)} \\ \xi_\uparrow^{*(a)} \\ \xi_\downarrow^{*(a)} \end{pmatrix} \quad (a = 1, 2). \tag{32}$$

Therefore, following relations are satisfied for the ZES

$$\xi_\uparrow^{(a)} = \xi_\uparrow^{*(a)} \ , \ \xi_\downarrow^{(a)} = \xi_\downarrow^{*(a)}. \tag{33}$$

If we expand the field operator of 1D Rashba semiconductor nanowire $\mathbf{\Psi} = (\hat{\psi}_\uparrow, \hat{\psi}_\downarrow, \hat{\psi}_\uparrow^\dagger, \hat{\psi}_\downarrow^\dagger)^T$ only by remaining ZES ignoring the high energy state, we obtain

$$\mathbf{\Psi} = \sum_{a=1,2} \gamma^{(a)} \begin{pmatrix} \xi_\uparrow^{(a)} \\ \xi_\downarrow^{(a)} \\ \xi_\uparrow^{*(a)} \\ \xi_\downarrow^{*(a)} \end{pmatrix}. \tag{34}$$

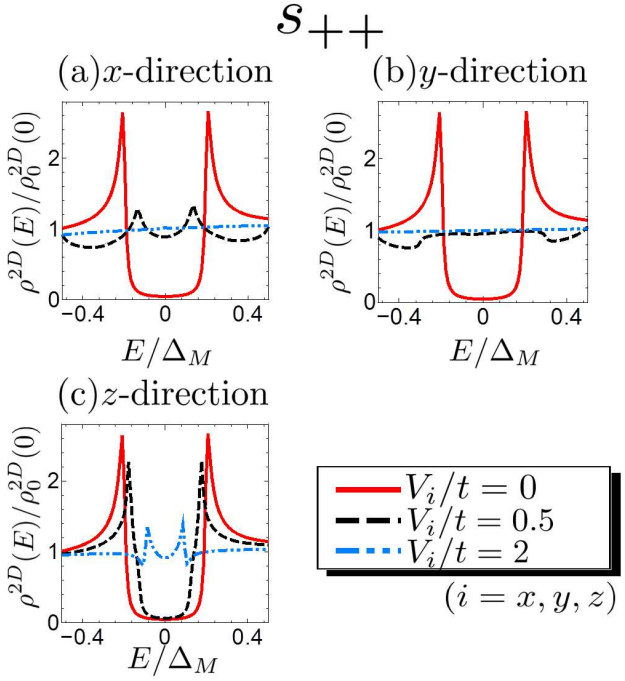

Fig. 12. (a)(b)(c)Normalized LDOS of a 2D Rashba semiconductor layer on s_{++}-wave superconductor with the Zeeman field $V_i/t=0$ (solid line), $V_i/t=0.5$ (dashed line), and $V_i/t=2$ (dot-dashed line) in (a)x-direction, (b)y-direction, (c)z-direction, and respectively. LDOS is normalized by its values in the normal state at $E=0$.

with real Majorana operator $\gamma^{(a)}$ satisfying $\gamma^{(a)\dagger}=\gamma^{(a)}$. We can introduce spin operator as follows:[75]

$$S_\alpha \equiv \frac{1}{4}[\hat{\psi}_i(\sigma_\alpha)_{ij}\hat{\psi}_j^\dagger - \hat{\psi}_i^\dagger(\sigma_\alpha^T)_{ij}\hat{\psi}_j] \tag{35}$$

From Eqs. (33) and (34), we can find that $S_x=0$, S_z=0, and $S_y\neq 0$. This means that the spin of zero energy Majorana edge state is not coupled with the Zeeman field applied in the x, z-directions but can be coupled with that in the y-direction. It is an Ising like character of Majorana edge state.[49,75,76] This result is consistent with the anisotropic response of the Zeeman field discussed in previous section.

4.2 2D case

In 2D case, the chiral operator defined in 1D, Γ^{1D} satisfies

$$(\Gamma^{1D})^\dagger \mathcal{H}_i^{2D}(k_x,k_y)\Gamma^{1D} = -\mathcal{H}_i^{2D}(k_x,-k_y). \tag{36}$$

Therefore, only at $k_y=0,\pi$, $\mathcal{H}_i^{2D}(k_x,k_y)$ anti-commutes with Γ^{1D}. We can introduce a winding number by similar way in 1D for fixed $k_y=0$ or $k_y=\pi$. The resulting winding

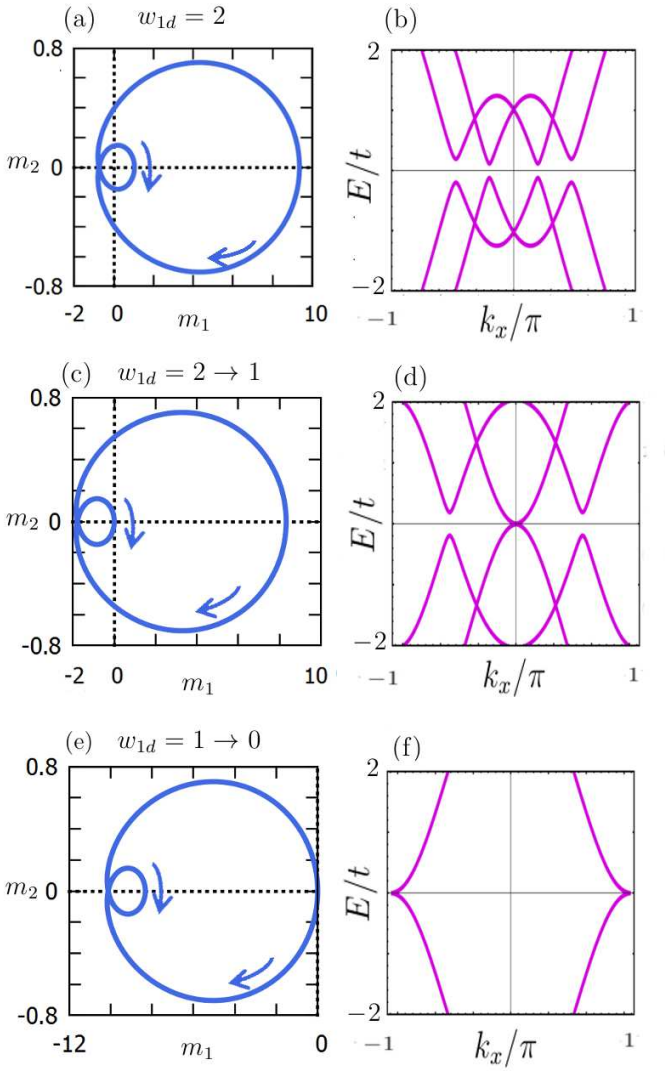

Fig. 13. (left)Trajectories of $\det q(k_x)$ and (right) energy dispersion of $\mathcal{H}_x^{\rm 1D}(k_x)$ (a)(b) without the Zeeman field, (c)(d) with the Zeeman field in the x-direction $V_x/t = 1.02$, and (e)(f)$V_x/t = 3.06$, respectively. m_1 denotes real part of $\det q(k_x)$ and m_2 is imaginary part of $\det q(k_x)$.

number at $k_y = 0(k_y = \pi)$ reads

$$w_{1d}(0(\pi)) = \frac{1}{2\pi i} \oint D^{-1} dD, \quad D = \det q(k_x, 0(\pi)), \tag{37}$$

where, $q(k_x, k_y) = (-2t\cos k_x - 2t\cos k_y - \mu)\sigma_0 + 2\lambda \sin k_x \sigma_y - i(\Delta_0 + 2\Delta_1 \cos k_x + 2\Delta_1 \cos k_y)\sigma_y$. The calculated winding numbers at $k_y = 0, \pi$ both in the case of $s_\pm$ and s_{++}-wave pairing is shown in Table III and IV with the applied Zeeman in the x and z-directions, respectively.

The arrows in the tables show the change of the topological numbers with the increase of the Zeeman field. We have confirmed that when the winding number is

Pairing	$(w_{1d}(0), w_{1d}(\pi))$
$s_{\pm}$	$(2,0) \to (1,1) \to (0,1) \to (0,0)$
s_{++}	$(0,0) \to (1,1) \to (0,1) \to (0,0)$

Table III. Changes of $(w_{1d}(0), w_{1d}(\pi))$ with the Zeeman field in x-direction in 2D. The critical values of the Zeeman field where winding number is changed are mentioned in Appendix.A

Pairing	$(w_{1d}(0), w_{1d}(\pi))$
$s_{\pm}$	$(2,0) \to (1,1) \to (0,1) \to (0,0)$
s_{++}	$(0,0) \to (1,1) \to (0,1) \to (0,0)$

Table IV. Changes of $(w_{1d}(0), w_{1d}(\pi))$ with the Zeeman field in z-direction in 2D. The critical values of the Zeeman field where winding number is changed are mentioned in Appendix.A

changed, the energy gap of the Hamiltonian at $k_y = 0$ or $k_y = \pi$ is closed. For $s_{\pm}$-wave pairing, there are three critical field V_{c1}, V_{c2}, and V_{c3}, where the energy gap at $k_y = 0$ or $k_y = \pi$ closes between $(w_{1d}(0), w_{1d}(\pi)) = (2,0)$ and (1,1), (1,1) and (0,1), and (0,1) and (0,0), respectively. These are $V_{c1} \sim 1.02$, $V_{c2} \sim 3.06$ and $V_{c3} \sim 5.10$ both for x-direction and z-direction cases. For s_{++}-wave pairing, the corresponding V_{c1}, V_{c2}, and V_{c3} given by $V_{c1} \sim 1.02$, $V_{c2} \sim 3.00$ and $V_{c3} \sim 5.00$ both for x-direction and z-direction cases. The w_{1d} changes (0,0), (1,1), (0,1) and (0,0) with the increase of Zeeman field. We can see that the results shown in Table III are consistent with the change of the number of the chiral edge modes at $k_y = 0$ and $k_y = \pi$ shown in Figs. 7 and 10. The difference between $s_{\pm}$ and s_{++}-wave only appears at the lower Zeeman field whether the topological state with $(w_{1d}(0), w_{1d}(\pi)) = (2,0)$ is realized or not. In the higher Zeeman field, since the number of the Fermi surface becomes one and the sign change of the pair potential does not occur any more. Thus, there is no essential difference between $s_{\pm}$ and s_{++}-wave pairings.

5. Conclusion

In this paper, we have studied the Majorana edge states and their topological properties of one-dimensional(1D) and two-dimensional(2D) Rashba semiconductor deposited on iron-based superconductor under the applied Zeeman field for various directions. Using the recursive Green's function method, we have calculated the LDOS and ARLDOS both for $s_{\pm}$ and s_{++}-wave pairings. We have discussed whether Majorana edge state

emerges or not based on the symmetry of the Hamiltonian. We have clarified Majorana edge states are protected by the mirror reflection symmetry and therefore it shows an anisotropic response to the directions of the applied Zeeman field. The resulting LDOS and winding numbers for $s_{\pm}$ and s_{++}-wave pairings are essentially different at the lower Zeeman field. These results serve as a guide to determine the pairing symmetry of iron-pnictide.

6. Acknowledgments

We would like to thank M. Sato for valuable discussions. This work was supported in part by a Grant-in Aid for Scientific Research from MEXT of Japan, "Topological Quantum Phenomena", Grants No. 22103005 and EU-Japan program "IRON SEA".

Appendix: Critical values of the Zeeman field

First, we focus on the 1D case. The eigenvalue energy of the Hamiltonian with the Zeeman field in the i-direction (i=x, z) is given by

$$\begin{aligned} E(k_x) &= \pm\sqrt{\alpha(k_x) \pm 2\sqrt{\beta(k_x)}} \\ \alpha(k_x) &= \xi_{k_x}^2 + |\Lambda(k_x)|^2 + V_i^2 + |\Delta(k_x)|^2 \\ \beta(k_x) &= \xi_{k_x}^2|\Lambda(k_x)|^2 + (\xi_{k_x}^2 + |\Delta(k_x)|^2)V_i^2, \end{aligned} \tag{A·1}$$

where, $\xi_{k_x} = -2t\cos k_x - \mu$, $\Lambda(k_x) = -i2\lambda_R \sin k_x$, $\Delta(k_x) = \Delta_0 + 2\Delta_1 \cos k_x$. The conditions of the gap closure is given as[77]

$$\xi_{k_x}^2 + |\Delta(k_x)|^2 = V_i^2 + |\Lambda(k_x)|^2, \;\; |\Delta(k_x)||\Lambda(k_x)| = 0 \tag{A·2}$$

From the second equation of (A·2), we obtain $k_x = 0$, π, $\mathrm{Cos}^{-1}(-\Delta_0/2\Delta_1)$ and put this k_x into the first equation, then we get the value of V_i. In the actual numerical calculations, we choose t=1, $\lambda_R = 0.5$, $\mu = -1$. $\Delta_0 = -0.2$ and $\Delta_1 = 0.2$ for $s_{\pm}$-wave pairing $\Delta_0 = 0.2$ and $\Delta_1 = 0.0$ for s_{++}-wave pairing.

We obtain the critical values of the Zeeman field for the gap closure. As for the $s_{\pm}$-wave case, critical values $V_i = V_{c1}$, $V_i = V_{c2}$ are $V_{c1}/t \sim 1.02$, $V_{c2}/t \sim 3.06$. As for the s_{++}-wave case, corresponding critical values are $V_{c1}/t \sim 1.02$ and $V_{c2}/t \sim 3.00$. Also, we confirm that at these critical values, winding number has a jump.

In 2D case, the eigenvalue energy of the Hamiltonian at $k_y = 0(\pi)$ with the Zeeman field in the i-directions (i=x, z)reads

$$E(k_x, 0(\pi)) = \pm\sqrt{\alpha(k_x, 0(\pi)) \pm 2\sqrt{\beta(k_x, 0(\pi))}}$$
$$\alpha(k_x, 0(\pi)) = \xi^2_{k_x,0(\pi)} + |\Lambda(k_x, 0(\pi))|^2 + V_i^2 + |\Delta(k_x, 0(\pi))|^2$$
$$\beta(k_x, 0(\pi)) = \xi^2_{k_x,0(\pi)}|\Lambda(k_x, 0(\pi))|^2$$
$$+(\xi^2_{k_x,0(\pi)} + |\Delta(k_x, 0(\pi))|^2)V_i^2, \tag{A·3}$$

where,

$$\xi_{k_x,0(\pi)} = -2t\cos k_x - 2t\cos(0(\pi)) - \mu, \tag{A·4}$$
$$\Lambda(k_x, 0(\pi)) = -i2\lambda_R \sin k_x + 2\lambda_R \sin(0(\pi)), \tag{A·5}$$
$$\Delta(k_x, 0(\pi)) = \Delta_0 + 2\Delta_1 \cos k_x + 2\Delta_1 \cos(0(\pi)). \tag{A·6}$$

The condition of gap closure is as follows.

$$\xi^2_{k_x,0(\pi)} + |\Delta(k_x, 0(\pi))|^2 = V_z^2 + |\Lambda(k_x, 0(\pi))|^2$$
$$|\Delta(k_x, 0(\pi))||\Lambda(k_x, 0(\pi))| = 0 \tag{A·7}$$

For the same set of parameters as in 1D case, we get the critical values for the gap closure at $k_y = 0, \pi$. In the case of $s_\pm$, critical values $V_i = V_{c1}$, $V_i = V_{c2}$ and $V_i = V_{c3}$ are given by $V_{c1}/t \sim 1.02$, $V_{c2}/t \sim 3.06$, and $V_{c3}/t \sim 5.10$, while in the case of s_{++}, $V_{c1}/t \sim 1.02$, $V_{c2}/t \sim 3.00$, and $V_{c3}/t \sim 5.00$. We also confirm that at these values, the winding number is changed.

References

1) N. Read and D. Green: Phys. Rev. B **61** (2000) 10267.

2) X.-L. Qi and S.-C. Zhang: Rev. Mod. Phys. **83** (2011) 1057.

3) J. Alicea: Rep. Prog. Phys. **75** (2012) 076501.

4) Y. Tanaka, M. Sato, and N. Nagaosa: J. Phys. Soc. Jpn. **81** (2012) 011013.

5) W. F.: Nature Phys. **5** (2009) 614.

6) D. A. Ivanov: Phys. Rev. Lett. **86** (2001) 268.

7) C. Nayak, S. H. Simon, A. Stern, M. Freedman, and S. Das Sarma: Rev. Mod. Phys. **80** (2008) 1083.

8) A. Y. Kitaev: Usp. Fiz. Nauk (Suppl.) **171** (2001) 131.

9) L. Fu and C. L. Kane: Phys. Rev. Lett. **100** (2008) 096407.

10) L. Fu and C. L. Kane: Phys. Rev. Lett. **102** (2009) 216403.

11) A. R. Akhmerov, J. Nilsson, and C. W. J. Beenakker: Phys. Rev. Lett. **102** (2009) 216404.

12) Y. Tanaka, T. Yokoyama, and N. Nagaosa: Phys. Rev. Lett. **103** (2009) 107002.

13) J. Linder, Y. Tanaka, T. Yokoyama, A. Sudbo, and N. Nagaosa: Phys. Rev. Lett. **104** (2010) 067001.

14) M. Veldhorst, M. Snelder, M. Hoek, T. Gang, V. K. Guduru, X. L. Wang, U. Zeitler, W. G. van der Wiel, A. A. Golubov, H. Hilgenkamp, and A. Brinkman: Nat. Mat. **11** (2012) 417.

15) J. R. Williams, A. J. Bestwick, P. Gallagher, S. S. Hong, Y. Cui, A. S. Bleich, J. G. Analytis, I. R. Fisher, and D. Goldhaber-Gordon: Phys.Rev.Lett. **109** (2012) 056803.

16) M. Sato and S. Fujimoto: Phys. Rev. B **79** (2009) 094504.

17) M. Sato, Y. Takahashi, and S. Fujimoto: Phys. Rev. Lett. **103** (2009) 020401.

18) J. D. Sau, R. M. Lutchyn, S. Tewari, and S. Das Sarma: Phys. Rev. Lett. **104** (2010) 040502.

19) J. Alicea: Phys. Rev. B **81** (2010) 125318.

20) Y. Oreg, G. Refael, and F. von Oppen: Phys. Rev. Lett. **105** (2010) 177002.

21) R. M. Lutchyn, J. D. Sau, and S. Das Sarma: Phys. Rev. Lett. **105** (2010) 077001.

22) J. Alicea, Y. Oreg, G. Refael, F. von Oppen, and M. Fisher: Nature Communications **7** (2011) 412.

23) V. Mourik, K. Zuo, S. Frolov, E. P. A. M. Bakkers, S. Plissard, and L. P. Kouwenhoven: Science **336** (2012) 1003.

24) M. Deng, C. Yu, G. Huang, M. Larsson, P. Caroff, , and H. Xu: Nano Lett. **12** (2012) 6414.

25) A. Das, Y. Ronen, Y. Most, Y. Oreg, and M. H. H. Shtrikman: Nature Phys. **8** (2012) 887.

26) H. O. H. Churchill, V. Fatemi, K. Grove-Rasmussen, M. T. Deng, P. Caroff, H. Q. Xu, and C. M. Marcus: Phys. Rev. B **87** (2013) 241401.

27) A. D. K. Finck, D. J. Van Harlingen, P. K. Mohseni, K. Jung, and X. Li: Phys. Rev. Lett. **110** (2013) 126406.

28) E. J. H. Lee, X.Jiang, M.Houzet, R. Aguado, C. M. Lieber, and S. D. Franceschi: Nature Nanotechnology **9** (2014) 79.

29) Y. Tanaka and S. Kashiwaya: Phys. Rev. Lett. **74** (1995) 3451.

30) S. Kashiwaya and Y. Tanaka: Rep. Prog. Phys. **63** (2000) 1641.

31) C. J. Bolech and E. Demler: Phys. Rev. Lett. **98** (2007) 237002.

32) K. T. Law, P. A. Lee, and T. K. Ng: Phys. Rev. Lett. **103** (2009) 237001.

33) D. J. P. Wimmer M., Akhmerov A. R. and B. C. W. J.: New J. Phys. **13** (2011) 053016.

34) C. W. J. Beenakker: Annu. Rev. Condens. Matter Phys. **4** (2013) 113.

35) L. Rokhinson, X. Liu, and J. Furdyna: Nat. Phys. **8** (2012) 795.

36) H.-J. Kwon, K. Sengupta, and V. Yakovenko: The European Physical Journal B - Condensed Matter and Complex Systems **37** (2004) 349.

37) A. P. Schnyder, S. Ryu, A. Furusaki, and A. W. W. Ludwig: Phys. Rev. B **78** (2008) 195125.

38) Y. Tanaka, T. Yokoyama, A. V. Balatsky, and N. Nagaosa: Phys. Rev. B **79** (2009) 060505.

39) A. Kitaev: AIP Conf. Proc. **1134** (2009) 22.

40) L. Fu and E. Berg: Phys. Rev. Lett. **105** (2010) 097001.

41) Y. Tanaka, Y. Mizuno, T. Yokoyama, K. Yada, and M. Sato: Phys. Rev. Lett. **105** (2010) 097002.

42) M. Sato, Y. Tanaka, K. Yada, and T. Yokoyama: Phys. Rev. B **83** (2011) 224511.

43) X.-L. Qi, T. L. Hughes, S. Raghu, and S.-C. Zhang: Phys. Rev. Lett. **102** (2009) 187001.

44) X.-L. Qi, T. L. Hughes, and S.-C. Zhang: Phys. Rev. B **81** (2010) 134508.

45) M. Sato: Phys. Rev. B **81** (2010) 220504.

46) J. C. Y. Teo and C. L. Kane: Phys. Rev. B **82** (2010) 11512.

47) S. Deng, L. Viola, and G. Ortiz: Phys. Rev. Lett. **108** (2012) 036803.

48) S. Nakosai, Y. Tanaka, and N. Nagaosa: Phys. Rev. Lett. **108** (2012) 147003.

49) S. Nakosai, J. C. Budich, Y. Tanaka, B. Trauzettel, and N. Nagaosa: Phys. Rev. Lett. **110** (2013) 117002.

50) Y. S. Hor, A. J. Williams, J. G. Checkelsky, P. Roushan, J. Seo, Q. Xu, H. W. Zandbergen, A. Yazdani, N. P. Ong, and R. J. Cava: Phys. Rev. Lett. **104** (2010) 057001.

51) S. Sasaki, M. Kriener, K. Segawa, K. Yada, Y. Tanaka, M. Sato, and Y. Ando: Phys. Rev. Lett. **107** (2011) 217001.

52) C. L. M. Wong and K. T. Law: Phys. Rev. B **86** (2012) 184516.

53) Y. Kim, J. Cano, and C. Nayak: Phys. Rev. B **86** (2012) 235429.

54) F. Zhang, C. L. Kane, and E. J. Mele: Phys. Rev. Lett. **111** (2013) 056402.

55) K. Ishida, Y. Nakai, and H. Hosono: Journal of the Physical Society of Japan **78** (2009) 062001.

56) I. I. Mazin, D. J. Singh, M. D. Johannes, and M. H. Du: Phys. Rev. Lett. **101** (2008) 057003.

57) K. Kuroki, S. Onari, R. Arita, H. Usui, Y. Tanaka, H. Kontani, and H. Aoki: Phys. Rev. Lett. **101** (2008) 087004.

58) H. Kontani and S. Onari: Phys. Rev. Lett. **104** (2010) 157001.

59) S. Onari and H. Kontani: Phys. Rev. Lett. **109** (2012) 137001.

60) Y. Yanagi, Y. Yamakawa, N. Adachi, and Y. Ono: Journal of the Physical Society of Japan **79** (2010) 123707.

61) A. A. Golubov, A. Brinkman, T. Y., M. I. I., and D. O. V.: Phys. Rev. Lett. **103** (2009) 077003.

62) A. V. Burmistrova, I. A. Devyatov, A. A. Golubov, K. Yada, and Y. Tanaka: Journal of the Physical Society of Japan **82** (2013) 034716.

63) M. Yamashiro, Y. Tanaka, and S. Kashiwaya: Phys. Rev. B **56** (1997) 7847.

64) M. Yamashiro, Y. Tanaka, Y. Tanuma, and S. Kashiwaya: J. Phys. Soc. Jpn. **67** (1998) 3224.

65) Y. Tanuma, K. Kuroki, Y. Tanaka, and S. Kashiwaya: Phys. Rev. B **64** (2001) 214510.

66) Y. Tanuma, K. Kuroki, Y. Tanaka, R. Arita, S. Kashiwaya, and H. Aoki: Phys. Rev. B **66** (2002) 094507.

67) F. Zhang, C. L. Kane, and E. J. Mele: Phys. Rev. Lett. **111** (2013) 056403.

68) Y. Ueno, A. Yamakage, Y. Tanaka, and M. Sato: Phys. Rev. Lett. **111** (2013) 087002.

69) C.-K. Chiu, H. Yao, and S. Ryu: Phys. Rev. B **88** (2013) 075142.

70) T. Morimoto and A. Furusaki: Phys. Rev. B **89** (2014) 035117.

71) M. Sato, A. Yamakage, and T. Mizushima: Physica E: Low-dimensional Systems and Nanostructures **55** (2014) 20 .

72) C. L. M. Wong, J. Liu, K. T. Law, and P. A. Lee: Phys. Rev. B **88** (2013) 060504.

73) X.G.Wen and A.Zee: Nuclear Physics B **316** (1989) 641.

74) S. Tewari and J. D. Sau: Phys. Rev. Lett. **109** (2012) 150408.

75) T.Mizushima, M.Sato, and K.Machida: Phys.Rev.Lett **109** (2012) 165301.

76) R. Shindou, A. Furusaki, and N. Nagaosa: Phys. Rev. B **82** (2010) 180505.

77) M.Sato: Phys.Rev.B **73** (2006) 214502.